The Astrophysical Journal, 809:62 (11pp), 2015 August 10 doi:10.1088/0004-637X/809/1/62

PAPER-64 CONSTRAINTS ON REIONIZATION. II. THE TEMPERATURE OF THE $z = 8.4$ INTERGALACTIC MEDIUM

Jonathan C. Pober[1,19], Zaki S. Ali[2], Aaron R. Parsons[2,3], Matthew McQuinn[4], James E. Aguirre[5], Gianni Bernardi[6,7,8], Richard F. Bradley[9,10,11], Chris L. Carilli[12,13], Carina Cheng[2], David R. DeBoer[3], Matthew R. Dexter[3], Steven R. Furlanetto[14], Jasper Grobbelaar[6], Jasper Horrell[6], Daniel C. Jacobs[15,19], Patricia J. Klima[10], Saul A. Kohn[5], Adrian Liu[2,16], David H. E. MacMahon[3], Matthys Maree[6], Andrei Mesinger[17], David F. Moore[5], Nima Razavi-Ghods[13], Irina I. Stefan[13], William P. Walbrugh[6], Andre Walker[6], and Haoxuan Zheng[18]

[1] Physics Dept., U. Washington, Seattle, WA, USA
[2] Astronomy Dept., University of California, Berkeley, CA, USA
[3] Radio Astronomy Lab., University of California, Berkeley, CA, USA
[4] Astronomy Dept., University of Washington, Seattle, WA, USA
[5] Dept. of Physics and Astronomy, University of Pennsylvania, Philadelphia, PA, USA
[6] Square Kilometre Array South Africa (SKA SA), Pinelands, South Africa
[7] Dept. of Physics and Electronics, Rhodes University, Grahamstown, South Africa
[8] Harvard-Smithsonian Center for Astrophysics, Cambridge, MA, USA
[9] Dept. of Electrical and Computer Engineering, University of Virginia, Charlottesville, VA, USA
[10] National Radio Astronomy Obs., Charlottesville, VA, USA
[11] Dept. of Astronomy, University of Virginia, Charlottesville, VA, USA
[12] National Radio Astronomy Obs., Socorro, NM, USA
[13] Cavendish Lab., Cambridge, UK
[14] Dept. of Physics and Astronomy, University of California, Los Angeles, CA, USA
[15] School of Earth and Space Exploration, Arizona State U., Tempe, AZ, USA
[16] Berkeley Center for Cosmological Physics, Berkeley, CA, USA
[17] Scuola Normale Superiore, Pisa, Italy
[18] Dept. of Physics, Massachusetts Institute of Technology, Cambridge, MA, USA

Received 2015 February 27; accepted 2015 June 26; published 2015 August 11

ABSTRACT

We present constraints on both the kinetic temperature of the intergalactic medium (IGM) at $z = 8.4$, and on models for heating the IGM at high-redshift with X-ray emission from the first collapsed objects. These constraints are derived using a semi-analytic method to explore the new measurements of the 21 cm power spectrum from the Donald C. Backer Precision Array for Probing the Epoch of Reionization (PAPER), which were presented in a companion paper, Ali et al. Twenty-one cm power spectra with amplitudes of hundreds of mK^2 can be generically produced if the kinetic temperature of the IGM is significantly below the temperature of the cosmic microwave background (CMB); as such, the new results from PAPER place lower limits on the IGM temperature at $z = 8.4$. Allowing for the unknown ionization state of the IGM, our measurements find the IGM temperature to be above $\approx$5 K for neutral fractions between 10% and 85%, above $\approx$7 K for neutral fractions between 15% and 80%, or above $\approx$10 K for neutral fractions between 30% and 70%. We also calculate the heating of the IGM that would be provided by the observed high redshift galaxy population, and find that for most models, these galaxies are sufficient to bring the IGM temperature above our lower limits. However, there are significant ranges of parameter space that could produce a signal ruled out by the PAPER measurements; models with a steep drop-off in the star formation rate density at high redshifts or with relatively low values for the X-ray to star formation rate efficiency of high redshift galaxies are generally disfavored. The PAPER measurements are consistent with (but do not constrain) a hydrogen spin temperature above the CMB temperature, a situation which we find to be generally predicted if galaxies fainter than the current detection limits of optical/NIR surveys are included in calculations of X-ray heating.

Key words: dark ages, reionization, first stars – galaxies: high-redshift – intergalactic medium

1. INTRODUCTION

Up until very recently, observational cosmology has lacked a direct probe of the conditions of the universe between the epoch of recombination and the birth of modern galaxies. Recent observations with the *Hubble Space Telescope* have found nearly a thousand putative galaxies at a redshift of 7 or above (see Bouwens et al. 2015 for a recent compilation), using the Lyman break drop-out technique. Narrow band searches for Lyα emitters have also proven successful at finding high-redshift galaxies (Ouchi et al. 2010; Tilvi et al. 2010; Hibon et al. 2011). However, these observations still principally detect the rare, most luminous galaxies, and cannot probe the population of more numerous, fainter galaxies.

One of the biggest unsolved questions in cosmology and galaxy formation is the issue of how early galaxies feed back into the universe and influence the formation of the next generation of galaxies. From a combination of cosmic microwave background (CMB; Larson et al. 2011; Planck Collaboration et al. 2015) observations and quasar absorption spectra measurements at high redshift (Fan et al. 2006; McGreer et al. 2015), we know that ultraviolet photons from the first luminous objects reionized the intergalactic medium

[19] National Science Foundation Astronomy and Astrophysics Postdoctoral Fellow.

(IGM) somewhere between redshifts ≈6 and 15. However, it has been determined that the observed high-redshift galaxy population cannot produce enough ionizing photons to complete the reionization of the universe before $z = 6$ (Choudhury et al. 2008; Finkelstein et al. 2012; Kuhlen & Faucher-Giguère 2012; Robertson et al. 2013). Therefore, to understand cosmic reionization, heating, and other feedback effects on the IGM, we require a probe of global conditions which captures the impact of the unobservable low-mass galaxies.

The 21 cm line of neutral hydrogen offers such a probe. By observing the 21 cm signal as a function of redshift, one can potentially trace the evolution of ionization, temperature, and density fluctuations on a cosmic scale (for reviews of 21 cm cosmology, see Furlanetto et al. 2006; Morales & Wyithe 2010 and Pritchard & Loeb 2012). At present, telescopes such as the LOw Frequency ARray (van Haarlem et al. 2013; Yatawatta et al. 2013)[20], the Murchison Widefield Array (MWA; Lonsdale et al. 2009; Bowman et al. 2013; Tingay et al. 2013)[21], and the Donald C. Backer Precision Array for Probing the Epoch of Reionization (PAPER; Parsons et al. 2010)[22] are conducting lengthy observational campaigns to detect the spatial power spectrum of 21 cm fluctuations from the Epoch of Reionization (EoR).

Initial measurements from a 32-element PAPER instrument in 2011 were recently used to place an upper limit on the 21 cm power spectrum at redshift 7.7 at a wavenumber of $k = 0.27\ h\mathrm{Mpc}^{-1}$ (Parsons et al. 2014). This upper limit was stringent enough to place constraints on the temperature of the IGM, requiring some mechanism for heating the intergalactic gas, and ruling out a universe in which the thermal evolution of the IGM was purely adiabatic since decoupling from the CMB. The goal of the present work is to expand on this analysis by using the more stringent upper limit from Ali et al. (2015) (hereafter, "Paper I") and by using a semi-analytic method to model the signal, allowing for a more complete exploration of the parameter space. This approach improves over Parsons et al. (2014) and Paper I, which constrained the spin temperature of the IGM by treating the brightness contrast between the spin and CMB temperatures as a multiplicative scalar on the amplitude of an analytic "patchy" reionization power spectrum. We review the measurements of Paper I in Section 2, and outline our methodology in Section 3. We present our constraints on the IGM temperature in Section 4, and discuss their physical implications in Section 5. We conclude in Section 6. Unless otherwise stated, all calculations assume a flat ΛCDM universe with $\Omega_m = 0.27$, $\Omega_\Lambda = 0.73$, $n_s = 0.96$, $\sigma_8 = 0.82$, and $h = 0.7$.

2. DATA AND MEASUREMENTS

The power spectrum measurements presented in Paper I represent a substantial improvement over the previous limits from PAPER in Parsons et al. (2014). While the previous measurements placed an upper limit of $\Delta^2(k) \leqslant (41\ \mathrm{mK})^2$ at $k = 0.27\ h\mathrm{Mpc}^{-1}$ and $z = 7.7$, the new limits from Paper I are significantly lower: $\Delta^2(k) \leqslant (22.4\ \mathrm{mK})^2$ over the range $0.15 < k < 0.5\ h\mathrm{Mpc}^{-1}$ at $z = 8.4$. This factor of 2 reduction (a factor of 4 in the temperature-squared units of the power spectrum) is the result of a large number of improvements over the previous analysis. The measurements in Paper I come from a 64-element PAPER array, as opposed to the 32-element array used in Parsons et al. (2014). There are also several significant changes to the data processing and analysis compared with that in Parsons et al. (2014). First, the application of the Omnical[23] redundant calibration package (Zheng et al. 2014) to the visibility data substantially improves the calibration and reduces the variance among measurements from physically redundant baselines. Second, the application of optimal fringe rate filtering has the effect of upweighting higher signal-to-noise regions on the sky and can limit the contamination from foreground emission at the northern and southern horizons. Finally, an improved power spectrum estimator using the optimal quadratic estimator formalism (Tegmark 1997; Liu & Tegmark 2011; Dillon et al. 2013) in conjunction with the delay spectrum approach (Parsons et al. 2012b) is used to downweight spectral eigenmodes that show significant foreground contamination. In a significant change from the Parsons et al. (2014) analysis, only the covariance between frequency channels within a single baseline's measurements is used in the weighting, as opposed to the covariance removal techniques that focused on inter-baseline covariance. See Paper I for a detailed description of each of these three new techniques.

The new power spectrum measurements from Paper I are shown in Figure 1 (equivalent to Figure 18 in Paper I). The left hand panel shows $P(k)$ in $\mathrm{mK}^2(h^{-1}\mathrm{Mpc})^3$, while the right hand panel plots the dimensionless power spectrum $\Delta^2(k)$ in mK^2. In both panels, black points represent the new measurements with 2σ error bars derived from bootstrapping, while vertical dashed black lines represent the nominal horizon limit, beyond which there should be no contamination from flat spectrum foreground emission (Parsons et al. 2012b; Pober et al. 2013). Also shown in the right hand panel are the expected theoretical 2σ noise limit (i.e., 95% of points should fall under this line if the measurements are consistent with thermal noise; dashed-cyan), a model 21 cm power spectrum at 50% ionization from Lidz et al. (2008; magenta), and three previous upper limits on the 21 cm signal: the Giant Metrewave Radio Telescope measurement at $z = 8.6$ (Paciga et al. 2013; yellow triangle); the MWA measurement at $z = 9.5$ (Dillon et al. 2014; purple triangle); and the Parsons et al. (2014) measurement (green triangle).

3. METHODOLOGY

As a way of placing these results in the context of a large and uncertain parameter space, we identify two parameters as being the dominant contributors to 21 cm power spectra with amplitudes at the level of the PAPER constraints: the average spin temperature of the emitting (i.e., neutral) gas—which at these redshifts is set by the kinetic temperature of the gas—and the average neutral fraction. To understand the physical conditions under which these two parameters drive the 21 cm power spectrum, it is worthwhile to keep the brightness temperature contrast between the 21 cm signal and the CMB,

[20] http://www.lofar.org
[21] http://www.mwatelescope.org
[22] http://eor.berkeley.edu
[23] https://github.com/jeffzhen/omnical

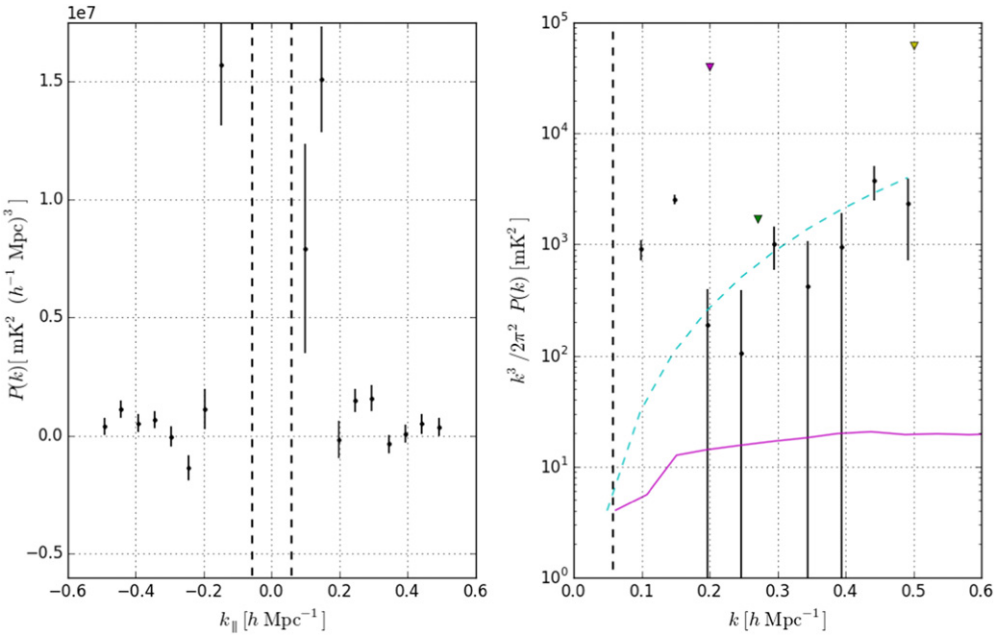

Figure 1. Left: the measured $P(k)$ in units of mK^2(h^{-1}Mpc)^3 over both positive and negative line of sight wavenumber $k_\parallel$. Right: the dimensionless power spectrum $\Delta^2(k) = \frac{k^3}{2\pi^2}P(k)$ in units of mK^2 vs. $|k|$. In both panels, black points represent the new measurements with 2σ error bars derived from bootstrapping, while black dashed lines represent the nominal horizon limit to flat spectrum foreground emission. Also shown in the right hand panel are the expected theoretical 2σ upper bounds of a noise-dominated measurement (dashed cyan), a model 21 cm power spectrum at 50% ionization from Lidz et al. (2008) (magenta), and three previous upper limits on the 21 cm signal: the Giant Metrewave Radio Telescope measurement at $z = 8.6$ (Paciga et al. 2013; yellow triangle); the MWA measurement at $z = 9.5$ (Dillon et al. 2014; purple triangle); and the Parsons et al. (2014) measurement (green triangle).

δT_b, in mind:

$$\delta T_b(\nu) \approx 9 x_{H\,I}(1+\delta)(1+z)^{\frac{1}{2}} \times \left[1 - \frac{T_{CMB}(z)}{T_S}\right]\left[\frac{H(z)/(1+z)}{dv_\parallel/dr_\parallel}\right] \text{mK}, \quad (1)$$

where $x_{H\,I}$ is the global neutral hydrogen fraction, z is the redshift, T_{CMB} is the temperature of the CMB, T_S is the spin temperature, $H(z)$ is the Hubble parameter, and $dv_\parallel/dr_\parallel$ is the gradient of the proper velocity along the line of sight (Furlanetto et al. 2006). It is worth explicitly stating that all the terms in Equation (1) can have different values at different spatial locations in the universe. When we refer to the *morphology* of, e.g., the ionization or spin temperature field, we are referring to the spatial distribution of the fluctuations in these quantities. We often quantify the statistics of these fluctuations in cosmological Fourier space using a power spectrum. If we define a fractional brightness temperature perturbation, $\delta_{21}(\boldsymbol{x}) \equiv [\delta T_b(\boldsymbol{x}) - \delta\bar{T}_b]/\delta\bar{T}_b$, the power spectrum, $P(\boldsymbol{k})$, is given by the ensemble average of the square of the spatial Fourier transform of this perturbation:

$$\left\langle \tilde{\delta}_{21}(\boldsymbol{k})\tilde{\delta}_{21}(\boldsymbol{k}')\right\rangle \equiv (2\pi)^3\delta(\boldsymbol{k}-\boldsymbol{k}')P(\boldsymbol{k}), \quad (2)$$

where the unsubscripted δ is a Dirac delta function.

Using these relations as a framework, we can now discuss the impact of our two principal parameters on the 21 cm power spectrum.

3.1. Spin Temperature

In the brightness temperature δT_b, the spin temperature enters as a ratio with the CMB temperature: $[1 - T_{CMB}(z)/T_S]$. If the spin temperature is much larger than the CMB temperature, this term saturates at a value of 1. It is often assumed during reionization that the spin temperature is already very large (e.g., Furlanetto 2006; Pritchard & Loeb 2008; Pober et al. 2014). It is thought that the emission of ultraviolet photons from the first luminous objects couples the spin temperature to the kinetic gas temperature field through the Wouthuysen–Field effect (Wouthuysen 1952; Field 1958).[24] And, in most models of early star and galaxy formation, the kinetic gas temperature has been raised to a very high level through heating from X-rays from the first high-mass X-ray binaries (HMXBs). (Recent work by Fialkov et al. 2014 has called this last statement into question, motivating the "cold" reionization scenarios we consider here.) However, it is clear that a very low value of the spin temperature—as can occur if X-ray heating is inefficient—can make the relevant term in the 21 cm brightness temperature (Equation (1)) large and negative, meaning the hydrogen gas is seen in absorption relative to the CMB. It is worth stressing that in our model T_S corresponds to the mass-averaged spin temperature. Like the ionization and density fields, the spin temperature also fluctuates spatially and contributes to the overall 21 cm power

[24] Using Equation (7) from McQuinn & O'Leary (2012), we estimate that a star formation rate density of $2.5 \times 10^{-3}\,M_\odot$ Mpc^{-3} yr^{-1} is necessary for the Wouthuysen–Field effect to couple the spin and color temperatures in the IGM by $z = 8.4$. The observed high redshift star formation rate density is nearly an order of magnitude higher than this value (Bouwens et al. 2015; McLeod et al. 2015), making the assumption that the spin temperature is equivalent to the kinetic temperature of the gas a valid one.

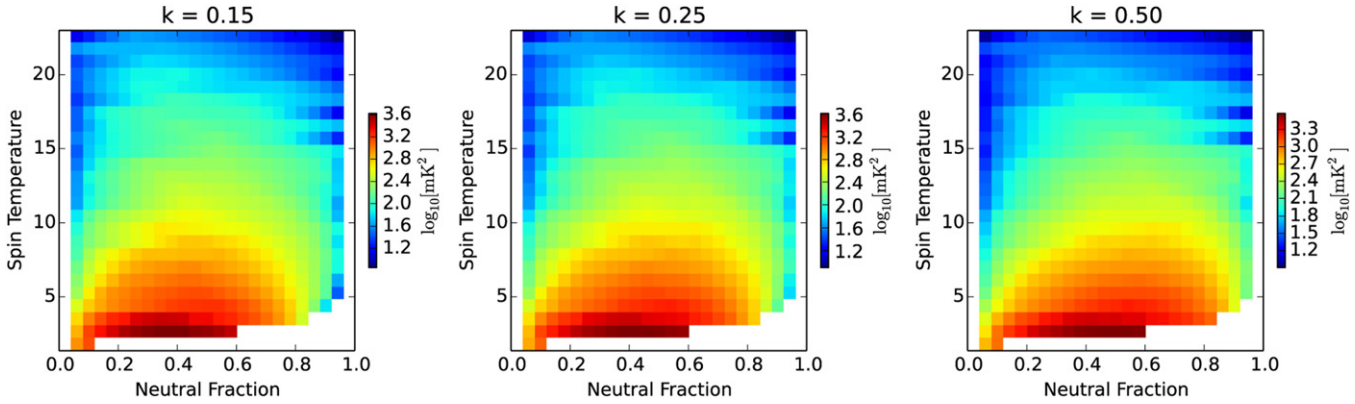

Figure 2. Power spectrum values in $\log_{10}$ mK^2 for different combinations of T_S and $x_{H\,I}$ at $z = 8.4$; the three panels show the value at $k = 0.15$, 0.25, and 0.50 hMpc^{-1}, respectively. It is clear that the power spectrum is relatively flat in k, with the brightest values occurring at very low spin temperatures. The sharp drop off in power above $T_S = 20$ K is expected; these spin temperatures are approaching the CMB temperature at $z = 8.4$, and as can be seen from Equation (1) for the brightness temperature, there is little to no 21 cm signal when the spin and CMB temperatures are comparable. (Some interpolation artifacts can also be seen at low and high neutral fractions for the larger spin temperatures; these features occur where the `21cmFAST` simulations give few data points. These artifacts have no effect on the conclusions of this work, which are concerned with the brighter power spectra at lower T_S where the space is well-sampled.)

spectrum. As we discuss below, we do not vary the morphology of the spin temperature fluctuations in our simulations, but rather vary only the total intensity of heating, effectively scaling the global temperature field.

3.2. Neutral Fraction

The evolution of the shape of 21 cm power spectrum as reionization proceeds is largely driven by the evolution in the neutral fraction, $x_{H\,I}$, and its spatial fluctuations, $\delta x_{H\,I}$. Simulations have shown that neutral fraction largely serves as a time coordinate during reionization; put another way, the shape (and, to a lesser degree, amplitude) of the power spectrum can largely be mapped one-to-one to the global neutral fraction, independent of the redshift at which the neutral fraction actually occurs (McQuinn et al. 2006; Lidz et al. 2008; Zahn et al. 2011; Pober et al. 2014). (It is worth noting that these earlier simulations were run under the assumption of $T_S \gg T_{CMB}$, but we find in our current simulations that the neutral fraction remains the principal factor in determining the shape of the 21 cm power spectrum even when this assumption is relaxed.)

3.3. Modeling Framework

The basic approach of this work is to explore the 21 cm power spectra that occur in the two-dimensional parameter space of (T_S, $x_{H\,I}$). Paper I explores this parameter space using a toy, analytic model for the ionization fluctuation power spectrum from "patchy" reionization: $\Delta^2_i(k) = (x_{H\,I} - x^2_{H\,I})/\ln(k_{max}/k_{min})$, and scaling its amplitude to model the effects of a globally cold spin temperature (Parsons et al. 2012a, 2014). We undertake a more physically motivated mapping of this space, using the publicly available `21cmFAST`[25] code v1.04 (Mesinger & Furlanetto 2007; Mesinger et al. 2011). Since each run of this code gives a full ionization history, we need to vary only the spin temperature as a function of neutral fraction, which we accomplish by varying the X-ray production efficiency, ζ_X. By effectively lowering the number of X-rays produced per stellar baryon, we reduce the rate at which the gas is heated, allowing us to produce power spectra for a large number of low spin temperatures. Thus, we use the new PAPER observations to place constraints on the relative timing of the EoR and X-ray heating epochs: the IGM can not be too cold outside of the cosmic H II patches, because the resulting 21 cm power would be too large at $z \approx 8.4$. Our methodology strives to quantify this statement, using fiducial EoR and X-ray heating models (all parameters other than ζ_X in `21cmFAST` are kept at their default fiducial values) and varying their relative timing.

In our simulations, we assume that the galactic X-ray luminosities follow a power law with a spectral energy index of 1.5, down to photon energies of $h\nu \geqslant 0.2$ keV. These values are consistent with *Chandra* observations of local, star-forming galaxies (Mineo et al. 2012a, 2012b), whose soft X-ray luminosities (relevant for heating the IGM) have comparable contributions from hot ISM emission and HMXBs. Pacucci et al. (2014) recently showed that the shape of the SED of early galaxies can impact the large-scale 21 cm signal during X-ray heating, by up to a factor of $\sim$ few. As explained below however, here we are most sensitive to the relative timing of the EoR and X-ray heating epochs, which can impact the large-scale 21 cm power by factors of $\sim$100 (Christian & Loeb 2013; Mesinger et al. 2014).

We use `21cmFAST` to calculate the ionization histories and associated power spectra for twelve values of ζ_X between 0 to 2×10^{56} (roughly 0–0.4 X-ray photons per stellar baryon). Each run produces 82 redshift outputs spanning the range $z = 6.14$ to $z = 34.51$. We then interpolate power spectra across the 3D space (T_S, $x_{H\,I}$, k). However, these simulations do not regularly cover this space; since the simulations start at such high redshift, there are significantly more data points at high neutral fractions than low. However, in the range where the PAPER constraints are significant, we have data points spaced by $\sim$0.6 K in T_S and $\sim$0.05 in neutral fraction.

Slices through this space at $k = 0.15$, 0.25, and 0.50 hMpc^{-1} are shown in Figure 2. As expected, the brightest power spectra occur at low spin temperatures. The drop-off in ampltiudes at high and low neutral fractions is also straightforward to understand. At high neutral fractions, the spatial distribution of $x_{H\,I}$ is relatively uniform, and this term does not add appreciable power to the power spectrum; the predominant contribution comes from density (δ) fluctuations, which have a

[25] http://homepage.sns.it/mesinger/DexM___21cmFAST.html

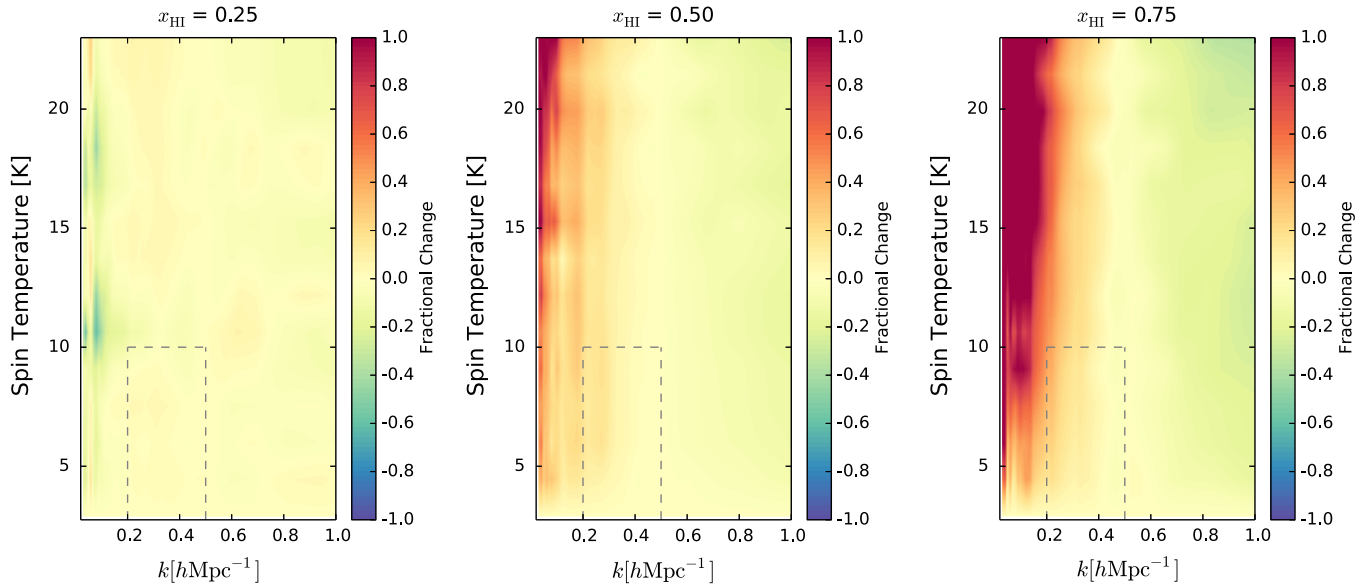

Figure 3. Fractional change in the 21 cm power shape caused by spin temperature fluctuations as a function of global spin temperature (i.e., heating efficiency). The three panels show different neutral fractions $x_{\rm H\,I} = 0.25$ (*left*), $x_{\rm H\,I} = 0.5$ (*center*), and $x_{\rm H\,I} = 0.75$ (*right*). In the regime where the PAPER constraints apply ($0.2\,h\mathrm{Mpc}^{-1} < k < 0.5\,h\mathrm{Mpc}^{-1}$, $T_{\rm S} < 10$ K, marked with the dotted lines), varying spin temperature fluctuation morphology changes the power spectrum shape by $\sim$ 10% or less.

smaller amplitude. At low neutral fractions, the lack of neutral hydrogen leads to an overall absence of the 21 cm signal. At the mid-point of reionization ($x_{\rm H\,I} \approx 0.5$), however, large ionized bubbles constrast strongly with predominantly neutral regions, leading to large spatial fluctuations in the $x_{\rm H\,I}$ field and a large 21 cm power spectrum amplitude.

One of the motivations for using such an approach is the elimination of redshift as a parameter to be explored.[26] While one of the principal goals of early 21 cm experiments is to determine the evolution of the cosmic neutral fraction as a function of redshift, the level of the current PAPER upper limit does not allow for such an analysis. And, while the PAPER measurement is at only one redshift, this method allows us to use that measurement to place constraints on the spin temperature without knowing the neutral fraction at $z = 8.4$. The other main benefit of this approach is that it eliminates the need to run simulations which only vary what are effectively "timing" parameters in the `21cmFAST` code: parameters that change the redshift at which specific neutral fractions occur, while having little to no effect on the shape or amplitude of the power spectrum at fixed neutral fraction.

3.4. Effect of Other Parameters

The exact shape and amplitude of the 21 cm power spectrum is the result of a rich combination of astrophysics and cosmology, which is difficult to fully map out in any parameter space, let alone a three-dimensional one. In this section, we consider the effects of parameters other than the spin temperature and neutral fraction on the 21 cm power spectrum. When the IGM is cold relative to the CMB, we find that these other effects are sub-dominant, amounting to relatively small corrections to our quantitative results. The reader primarily interested in the IGM temperature limits placed by PAPER can skip to Section 4.

In simulations where $T_{\rm S} \gg T_{\rm CMB}$, the properties of the sources contributing to reionization are the dominant drivers of the 21 cm power spectrum and its evolution. In the `21cmFAST` code, these parameters include ζ, the ionizing efficiency of galaxies—which we find has no effect on the shape or amplitude of the power spectrum—and the minimum virial temperatures of the halos that can produce both ionizing or X-ray photons—which has a small effect on the power spectrum relative to the global spin temperature, but predominantly changes the timing of reionization and/or heating (Mesinger & Furlanetto 2007; Mesinger et al. 2011; Pober et al. 2014). Simulations which spanned the range of reasonable values for the minimum virial temperature of ionizing halos in Pober et al. (2014) only varied the peak power spectrum brightness at 50% ionization between $\approx$10 and 30 mK^2. This scale is far below the power spectrum amplitudes achievable with a cold IGM, which can range from several hundred to several thousand mK^2, as seen in Figure 2.

Driving the effective dominance of the spin temperature in setting the amplitude of these strong ($\sim$thousand mK^2) 21 cm signals is the contrast of the cosmic ionized patches ($\delta T_{\rm b} \approx 0$ mK) with the cold ($\delta T_{\rm b} \gtrsim -200$ mK), neutral patches (Christian & Loeb 2013; Mesinger et al. 2014; Parsons et al. 2014). We note however that the uncertainty in the precise morphological structure of the ionization and temperature fluctuations does quantitatively impact our constraints. Our approach largely assumes that the contribution of spatial fluctuations in the spin temperature to the 21 cm power spectrum does not vary with the effectiveness of X-ray heating. One expects that spin temperature fluctuations would be small if heating is inefficient and would grow larger with stronger heating. We quantify the change in the shape of the 21 cm power spectrum versus heating efficiency in Figure 3. For low neutral fractions, the change is small ($\sim$10%) regardless of spin

[26] In order to correct for the effects of redshift—`21cmFAST` produces ionization histories where each neutral fraction corresponds to a specific redshift, whereas we want to compare to measurements specifically at $z = 8.4$—we scale each power spectrum relative to the CMB temperature at $z = 8.4$: $P(k, z = 8.4) = P_{\texttt{21cmFAST}}(k, z) * \left(\frac{T_{\rm S} - T_{\rm CMB}(z=8.4)}{T_{\rm S} - T_{\rm CMB}(z)}\right)^2$.

temperature. At higher neutral fractions, spin temperature fluctuations increase the 21 cm power spectrum at large scales ($k < 0.2\ h\mathrm{Mpc}^{-1}$) by factors of as much as 3 when heating is relatively efficient and the global spin temperature is high. We also see a decrease in 21 cm power by factors of up to ∼30% at smaller scales ($k > 0.6\ h\mathrm{Mpc}^{-1}$). However, in the regime constrained by the PAPER measurements (scales $0.2\ h\mathrm{Mpc}^{-1} < k < 0.5\ h\mathrm{Mpc}^{-1}$, and, as shown subsequently, spin temperatures less than 10 K, demarcated by the dotted lines), we find spin temperature fluctuations introduce typical changes of ∼10% or less. Therefore, our approximation of a spin temperature field morphology independent of heating efficiency should introduce only small uncertainties into our constraints. This result largely confirms the findings of Pritchard & Furlanetto (2007), and validates the approach of Paper I to use the global spin temperature as a multiplicative scalar for the overall power spectrum amplitude.

Our methodology also implicitly assumes that the contribution to the overall power spectrum from the density, velocity, and temperature fluctuation terms that contribute to $\Delta^2(k)$ changes minimally over the redshift range spanned by the simulations. The ionization history simulated by `21cmFAST` is in principle independent of the heating history; in our simulations, the IGM is 90% neutral at $z = 12.5$, 50% neutral at $z = 9.5$, and 10% neutral at $z = 8$. In extrapolating all neutral fractions to $z = 8.4$, we have assumed that the ionization field provides the dominant contribution to the power spectrum across this redshift range, and that the fractional contribution of the density and velocity fields to the power spectrum evolves relatively slowly. This is in general a good assumption for neutral fractions between ≈10% and 90%, which are achieved over a narrow redshift range, but makes the interpretation of high and low neutral fractions (where our constraints are the poorest) more questionable. We do expect the spin temperature fluctuations to grow more important at lower redshifts (the temperature of an overdense region grows faster than its density), but this is also a relatively small effect over the redshift range we extrapolate from.

One additional free parameter in `21cmFAST` is the mean free path of ionizing photons through the IGM, which primarily accounts for the unresolved, self-shielded pockets of neutral gas that limit the extent of H II regions. This parameter has been shown to alter the shape of the 21 cm power spectrum (Pober et al. 2014; Sobacchi & Mesinger 2014; Greig & Mesinger 2015), but principally only on the largest scales, at which the PAPER measurements are limited by residual foreground emission.

These caveats do suggest that our quantitative results should not be too strictly interpreted, as we have neglected several effects that could change the constraints by ∼ tens of percent. Given the scale of the current PAPER upper limit and the range of k modes measured, however, working in the two-dimensional parameter space of spin temperature and neutral fraction remains a well-motivated approach.

4. RESULTS

At each position in the (T_S, $x_{H\,I}$) space plotted in Figure 2, we calculate the probability of getting the measurements shown in Figure 1 given our model `21cmFAST` power spectrum at those values of (T_S, $x_{H\,I}$). We calculate the joint likelihood across all values of k measured by PAPER. As described in Paper I, the 2σ error bars plotted in Figure 1 are calculated from bootstrapping; here, we assume they follow a Gaussian distribution to allow for analytic calculation of the likelihood. We also make the conservative choice to treat all our measurements as upper limits on the 21 cm signal so that we only exclude models which predict *more* power than we observe. The PAPER measurements clearly detect non-zero power at several wavemodes; if treated as detections of the 21 cm signal, these points would exclude, e.g., the model power spectrum in Figure 1 for being too faint. Therefore, when calculating the likelihood that our data are consistent with a given model, we exclude any constraints from points brighter than the model prediction.

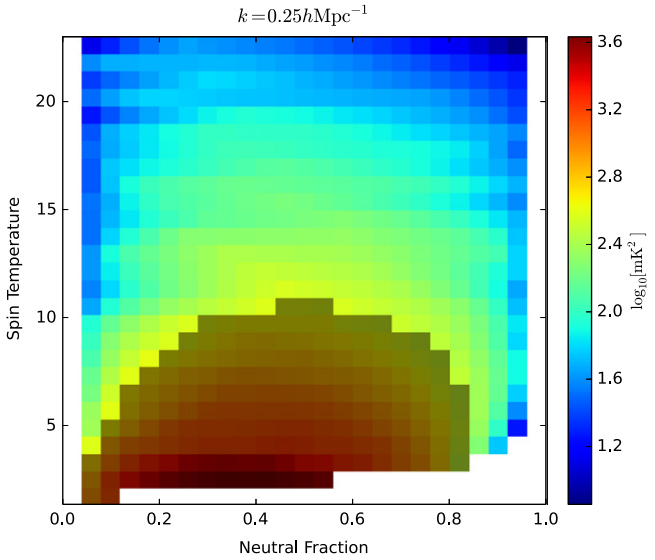

Figure 4. Constraints on the IGM spin temperature as a function of neutral fraction based on the 2σ upper limits from the PAPER measurements; regions excluded at greater than 95% confidence are shaded in gray. Plotted is a slice through our 3D (T_s, $x_{H\,I}$, k) space at the $k = 0.25\ h\mathrm{Mpc}^{-1}$, but the constraints are calculated from the joint likelihood across all k modes measured by PAPER.

The constraints produced by this analysis are shown in Figure 4. As expected, our measurements are inconsistent with very low spin temperatures, as these models produce the brightest power spectra. The exact spin temperatures ruled out by our data depend somewhat on the (currently unknown) neutral fraction in the IGM at $z = 8.4$. For neutral fractions between 10% and 85%, we can rule out spin temperatures below ≈5 K at 95% confidence. By narrowing the range of neutral fractions, our constraints grow more stringent: if the universe is between 15% and 80% neutral at $z = 8.4$, we rule out spin temperatures below ≈7 K, and for neutral fractions between 30% and 70%, we require T_S to be greater than ≈10 K. The explanation for the poorer constraints at the highest and lowest neutral fractions is straightforward: spatial fluctuations in the ionization field are small at the beginning and end of reionization, lowering the amplitude of the power spectrum, and allowing for a colder IGM to still be consistent with the data. If there is no heat injection into the universe, cosmological adiabatic cooling brings the gas temperature to 1.18 K at $z = 8.4$ (if thermal decoupling of the gas occurs at at $z = 200$). Assuming the Wouthuysen–Field effect has efficiently coupled the spin temperature of the hydrogen to the kinetic temperature of the gas, our measurements require a gas temperature ≈5–10 times larger than the minimum allowed by adiabatic cooling.

Comparing these results with those from the analytic toy model calculations from Paper I, we see general agreement, although our constraints are somewhat stronger. The calculation in Paper I does not include any of the physical effects of reionization; rather, it assumes a flat power spectrum between a minimum and maximum wavenumber and uses the integral constraint for a patchy reionization that $\int d\ \log\ k\ \Delta_i^2(k) = x_{\rm H\,I} - x_{\rm H\,I}^2$. The minimum and maximum wavenumbers roughly correspond to a range of ionized bubble scales; as they grow closer together, more power accumulates within a narrow range of wavenumbers. While it is difficult to directly compare this simple model to our semi-analytic results, it is reassuring to find results constraining a similar range of $T_{\rm S}$.

5. DISCUSSION

It is interesting to compare our constraints on the temperature of the $z = 8.4$ IGM with theoretical predictions. As stated previously, most models of early galaxy formation and reionization predict fairly efficient heating, such that the temperature of the IGM is much greater than that of the CMB by $z \lesssim 10$ (Furlanetto 2006; McQuinn & O'Leary 2012). Here, we consider two models that have the potential to result in low amounts of cosmic heating: an observationally based model, where we consider the heating produced by the currently observed high redshift galaxy population, and a more physical model, where we compare with predictions using the recently proposed reionization model from Robertson et al. (2015) (hereafter, R15). These two models are discussed in Sections 5.2 and 5.3, respectively.

We can estimate the heating we would expect by solving the differential equation demanded by energy conservation in an expanding universe:

$$\frac{dT_K}{dt} = -2H(z)T_{\rm K} + \frac{2}{3}\frac{\epsilon_{\rm X}}{k_{\rm B}n}, \tag{3}$$

where $T_{\rm K}$ is the kinetic temperature of the IGM, $k_{\rm B}$ is Boltzmann's constant, n is the number density of neutral gas particles, and $\epsilon_{\rm X}$ is the energy injected into the IGM per second per unit volume by X-ray sources (Furlanetto et al. 2006). To estimate $\epsilon_{\rm X}$, we use the star formation rate densities ($\dot{\rho}_{\rm SFR}$) measured from the observed high redshift galaxy population by Bouwens et al. (2015) and McLeod et al. (2015) and the local correlation between star formation and X-ray luminosity:

$$L_{\rm X} = 3.4 \times 10^{40} f_{\rm X} \frac{\rm SFR}{1 M_\odot\ {\rm yr}^{-1}}\ {\rm erg\ s}^{-1}, \tag{4}$$

where SFR is the star formation rate, and $f_{\rm X}$ is an unknown high redshift normalization factor (Grimm et al. 2003; Ranalli et al. 2003; Gilfanov et al. 2004). Equation (4) can be related to $\epsilon_{\rm X}$ by $\epsilon_{\rm X} = 3.4 \times 10^{40} f_{\rm X} f_{\rm abs}\, \dot{\rho}_{\rm SFR}$, where $f_{\rm abs}$ is the fraction of total X-ray emission that deposits heat into the IGM. Given $f_{\rm X}$, $f_{\rm abs}$, and $\dot{\rho}_{\rm SFR}(z)$, we can solve Equation (3) to predict the temperature of the IGM.

5.1. Parameter Uncertainties

Each of the three parameters described above is not well-determined at high redshift. Here we discuss the uncertainties in each before constructing models to span the range of uncertainties.

1. $f_{\rm X}$. Early measurements of the local star formation rate/X-ray luminosity correlation yielded, a value of $3.4 \times 10^{40} f_{\rm X} \frac{\rm SFR}{1 M_\odot\ {\rm yr}^{-1}}$ erg s^{-1} (Grimm et al. 2003; Gilfanov et al. 2004); $f_{\rm X}$ is a correction factor relative to these initial measurements. More recent measurements have suggested that the local $f_{\rm X}$ value is closer to 0.2 (Lehmer et al. 2010; Mineo et al. 2011, 2012a, 2012b), while the high-redshift value still has large uncertainties (Dijkstra et al. 2012). Fragos et al. (2013) model the redshift evolution of the HMXB population, and find that $f_{\rm X}$ may be up to 10 times higher than local, i.e., $f_{\rm X} = 2.0$, while observations from Cowie et al. (2012) find little to no redshift evolution in $f_{\rm X}$ up to $z \approx 6$. In this work, we consider $f_{\rm X}$ values which span the range 0.2–2.0.
2. $f_{\rm abs}$. X-rays heat the IGM by first photoionizing a neutral atom. The resultant fast electron then deposits a fraction of its energy into heating the IGM gas itself. The relative fraction of this ionization energy which goes into heating depends on the X-ray photon energy and the neutral fraction of the hydrogen gas (Shull & van Steenberg 1985; Chen & Kamionkowski 2004; Valdés & Ferrara 2008; Furlanetto & Stoever 2010). However, since we are concerned only with the temperature of the predominantly neutral regions in the IGM (as this gas is responsible for the 21 cm signal), the global ionization fraction is not the relevant quantity for determing the fraction of energy that goes to heating the gas. Rather, it is the small ionization fraction produced by X-rays which have penetrated into the neutral regions; in the limit of very small ionization fractions, a constant value of $f_{\rm abs} = 0.2$ is a good approximation (Valdés & Ferrara 2008).[27]

   Recently, Fialkov et al. (2014) suggested that previous heating calculations assumed too soft a spectra for X-ray emitters (specifically, HMXBs) at high redshift. Using a spectral model with fewer soft photons, they find the absorption of X-rays by the IGM can be reduced by as much as a factor of 5. Pacucci et al. (2014) argue the opposite: that the early galaxies have softer X-ray spectra due to (i) a contribution from the thermal emission from the hot interstellar medium (ISM), which is locally found to be comparable at the relevant energy range to that of the HMXBs (only the latter is used to motivate the scaling in Equation (4)); and (ii) lower column densities and metallicities of early galaxies compared to local ones, resulting in more soft X-rays escaping into the IGM. For robustness, we explore a broad parameter space, considering values of $f_{\rm abs}$ spanning the range 0.04–0.2 in our calculations.
3. *Star Formation Rate Density.* There has been some debate in the literature as to the evolution of the star formation rate density at high redshift. Modeling the star formation rate density redshift evolution as a power law, $\dot{\rho}_{\rm SFR} \propto (1+z)^{\alpha}$, Bouwens et al. (2015) and Oesch et al.

[27] The fact that we are considering cold reionization scenarios ensures the amount of ionization caused by X-rays must be small. For predominantly neutral gas, the ratio of X-ray energy injection contributing to ionization is no more than ~3 times that contributing to heating (Valdés & Ferrara 2008). An injection of $\sim 10^{-2}$ eV/atom as heat would raise the gas temperature to ~100 K, well outside of the cold IGM regime constrained by the PAPER measurements. Therefore, a maximum of $\sim 3 \times 10^{-2}$ eV/atom could have gone into ionizations, which could produce an ionization fraction no larger than $\sim 2 \times 10^{-3}$.

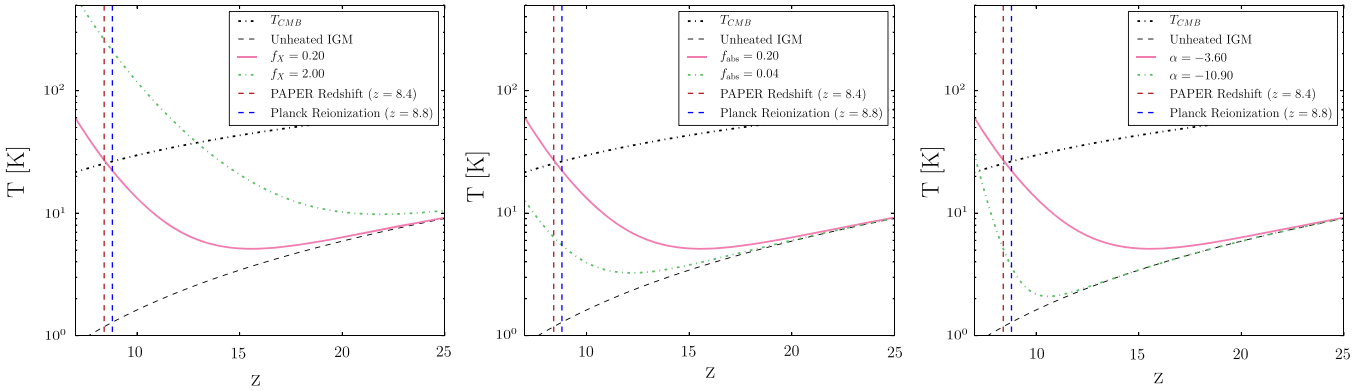

Figure 5. Dependence of evolution of the IGM temperature as a function of redshift on the uncertain parameters in the calculation: f_x (left), f_{abs} (middle), and α (right). In all panels, the solid pink curve plots our fiducial model with $f_X = 0.2$, $f_{abs} = 0.2$, and $\alpha = -3.6$. The dashed vertical red and blue lines show the redshift of the PAPER measurement ($z = 8.4$) and the *Planck* maximum likelihood redshift for an instantaneous reionization ($z = 8.8^{+1.7}_{-1.4}$), respectively. The black dashed curve shows the minimum gas temperature from adiabatic cooling, and the black dot–dashed curve shows the CMB temperature. All predictions are based on the assumption that the observed $z = 7$ galaxy population is providing the X-rays that heat the IGM.

(2014) find a very steep drop off of $\alpha = -10.9$ at high redshift. Other measurements from McLeod et al. (2015) find a much shallower evolution, $\dot{\rho}_{SFR} \propto (1+z)^{-3.6}$ (although the best fits come from a more complex functional form with a slightly steeper slope). We consider models using both these power law indices, although for our fiducial model we choose $\alpha = -3.6$, since a larger high redshift $\dot{\rho}_{SFR}$ seems necessary to produce the *Planck* optical depth (Planck Collaboration et al. 2015, R15). To set the overall scale of this power law, we set the star formation rate density at $z = 7$ to be $10^{-2}\, M_\odot$ Mpc^{-3} yr^{-1}, consistent with the observed values from Bouwens et al. (2015) and McLeod et al. (2015) (although a correction for extinction does result in slightly higher values).

The effect on the heating history from varying each parameter is plotted in Figure 5; the left hand panel shows the effect of changing f_X, the middle f_{abs}, and the right α. The parameters not being varied are held at fiducial values of $f_X = 0.2, f_{abs} = 0.2$, and $\alpha = -3.6$; in each panel, this fiducial model is plotted in solid pink. Also plotted is the expected gas temperature in the absence of any heating (black, dashed) and the CMB temperature (black, dot–dashed). Dashed vertical lines show the redshifts of the PAPER measurement ($z = 8.4$; red) and the *Planck* maximum likelihood instantaneous reionization redshift ($z = 8.8^{+1.7}_{-1.4}$; blue). The CMB temperature at $z = 8.4$ is 25.4 K; if the gas temperature is below the CMB temperature, then the 21 cm signal will be seen in absorption. We see that relative to our fiducial model, only an increased value of f_X heats the gas well above the CMB temperature, while choosing the minimum values for either f_{abs} or α can result in an IGM temperature well below the $\approx$10 K lower limit at $z = 8.4$ from the PAPER measurements.

5.2. Comparison with Observations

To better explore the parameter space, we plot the predicted $z = 8.4$ IGM temperature produced by the observed galaxy population versus both α and f_X in Figure 6. For the fiducial value of $f_{abs} = 0.2$ (left), we rule out very little parameter space, but do disfavor the combination of a steep α and low f_X. In general, however, the observed galaxies heat the IGM beyond both the realm ruled out by the PAPER measurements and the CMB temperature of 25.4 K. With a lower value of $f_{abs} = 0.04$, chosen to represent the harder X-ray spectra suggested by Fialkov et al. (2014), we rule out a significant region of parameter space (right panel of Figure 6). In this model, both the steepest slopes for models of $\dot{\rho}_{SFR}$ and the smallest values of f_X are excluded. However, there is still a large range of parameter space where the IGM temperature is heated above the limits set by PAPER.

Of course, the constraints we have placed on the parameters in our heating model can still be avoided by invoking other sources of heating—whether from an additional population of fainter, yet-undetected galaxies, or from other mechanisms such as active galactic nuclei and/or quasars (Volonteri & Gnedin 2009), shock heating (Gnedin & Shaver 2004; McQuinn & O'Leary 2012), or even dark matter annihilation (Evoli et al. 2014). It is often claimed that fainter galaxies than those observed are necessary to reionize the IGM (Choudhury et al. 2008; Finkelstein et al. 2012; Kuhlen & Faucher-Giguère 2012; Robertson et al. 2013; R15); our measurements also imply that fainter galaxies would be required to heat the IGM if X-ray heating turns out to be on the inefficient side of the currently allowed parameter space. The fact, however, that an additional galaxy population is required to complete reionization within the observationally allowed redshift range makes the constraints arising from the observed galaxy heating model used in this section relatively unphysical. If there are no fainter galaxies than those observed, it is implausible for the universe to be significantly ionized at $z = 8.4$ (although high values of the ultraviolet photon escape fraction from galaxies at high redshift could allow for reionization to be completed by the observed galaxy population). And, if the IGM is significantly neutral, the PAPER lower limit on T_S becomes much weaker (see Figure 4). However, if we remain agnostic about the source of ionizing photons, the PAPER measurements do place constraints on the sources heating the IGM, ruling out a range of models of X-ray heating.

5.3. Extrapolating the Luminosity Function

As noted above, galaxies fainter than those currently detected at high redshift are expected in most theoretical models, and are in fact necessary to complete the reionization

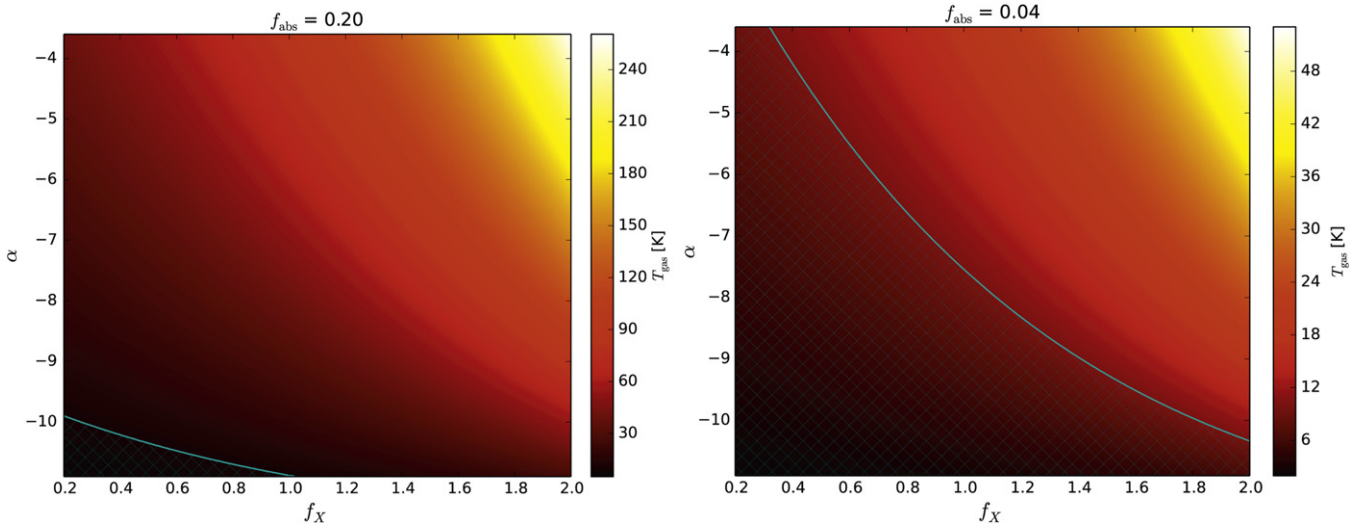

Figure 6. Predicted IGM temperature produced by the observed galaxy population as a function of the model parameters α and f_X. The hashed cyan regions are excluded based on the PAPER constraints that $T_{IGM} \gtrsim 10$ K (assuming the neutral fraction is between 30% and 70% at $z = 8.4$). Left: $f_{abs} = 0.20$. With the fiducial absorption coefficient, very little parameter space is ruled out. However, we disfavor a combination of a steep slope to the $\dot{\rho}_{SFR}(z)$ relation and lower value of f_X close to the locally measured value. Right: $f_{abs} = 0.04$, as suggested by Fialkov et al. (2014). A considerable amount of parameter space in the observed galaxy model is ruled out, disfavoring the local value of $f_X = 0.2$ and the steeper slope of $\dot{\rho}_{SFR}(z)$ of $\alpha = -10.9$. Even with this very low value of f_{abs}, there is still room for the observed galaxies alone to heat the IGM well above T_{CMB}.

of the universe by $z = 6$ (barring other significant contributors of ionizing photons; Choudhury et al. 2008; Finkelstein et al. 2012; Kuhlen & Faucher-Giguère 2012; Robertson et al. 2013; R15). While the analysis in Section 5.2 placed constraints on the heating that can be provided by only the observed galaxies, it is useful to explore a more self-consistent model, where we include the heating that would be generated by the galaxies necessary to reionize the universe. As a model, we use the maximum-likelihood star formation fit from R15, which uses the four-parameter fitting function of Madau & Dickinson (2014):

$$\dot{\rho}_{SFR}(z) = a_p \frac{(1+z)^{b_p}}{1 + \left[(1+z)/c_p\right]^{d_p}}, \quad (5)$$

with best fit values of[28] $a_p = 0.01376 \pm 0.001\ M_\odot\ \mathrm{yr}^{-1}\,\mathrm{Mpc}^{-3}$, $b_p = 3.26 \pm 0.21$, $c_p = 2.59 \pm 0.14$, and $d_p = 5.68 \pm 0.19$. These values fit the compilation of star formation rate densities in Madau & Dickinson (2014), but where each measured $\dot{\rho}_{SFR}$ value has been increased to include an extrapolation to fainter galaxies. Specifically, R15 take the measured galaxy luminosity function at each redshift and integrate down to $0.001L_*$ to produce a total estimate of star formation rate density at that redshift (where L_* is the characteristic luminosity of a galaxy). The value of $\dot{\rho}_{SFR}$ at $z = 7$ predicted by the R15 model is not significantly higher than the currently observed rates: $0.020^{+0.0029}_{-0.0025}\ M_\odot\ \mathrm{yr}^{-1}\,\mathrm{Mpc}^{-3}$ (compared with the value of $0.01\ M_\odot\ \mathrm{yr}^{-1}\,\mathrm{Mpc}^{-3}$ currently observed near this redshift), suggesting that half the galaxies necessary for reionization have already been observed. With fainter galaxies included in calculations of the IGM ionization history, the R15 model completes reionization by $z \approx 6$, and

[28] Note, however, that there exist correlations between these errors, and as such, the range of star formation rate histories allowed by R15 is smaller than one might naïvely calculate.

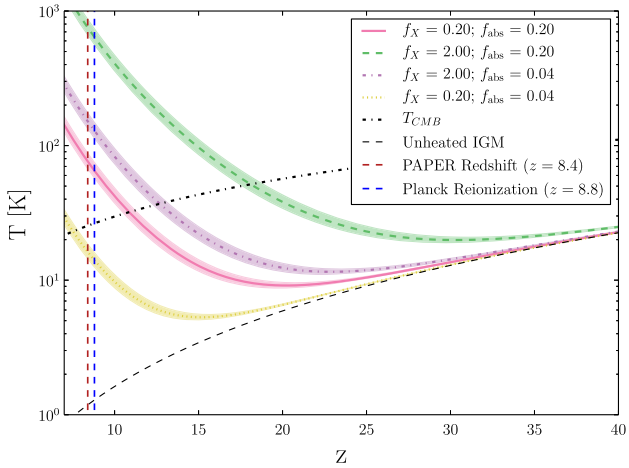

Figure 7. Predicted heating of the IGM from the R15 best fit star formation rate density evolution; our fiducial model is plotted in solid pink. Shaded regions around each curve correspond to 1σ uncertainties calculated from the 68% confidence regions in the R15 model. Even when the parameters are tuned for the weakest heating of the IGM, the model predicts gas temperatures above those ruled out by the PAPER lower limit.

produces an optical depth to reionization consistent with the *Planck* value (Planck Collaboration et al. 2015). The reionization history predicted by this model reaches 50% ionization at $z \approx 7.5$; at $z = 8.4$, the redshift of the PAPER measurements, this model predicts the universe is ≈70% neutral. See Figure 3 of R15 for the full predicted ionization history.

Figure 7 shows the IGM heating histories calculated from the R15 star formation rate density evolution model for all combinations of f_X and f_{abs} (α is not a free parameter of the model.) We see that even when tuned for the weakest heating ($f_X = 0.2, f_{abs} = 0.04$), the R15 model produces enough X-ray photons to bring the gas temperature above the lower limit of 10 K set by PAPER. (As argued in Fialkov et al. 2014,

this model does still produce a relatively cold reionization, with $T_{\rm gas} \approx T_{\rm CMB}$ at $z \approx 8$.) Our fiducial heating model of $f_{\rm X} = 0.2, f_{\rm abs} = 0.2$ heats the gas to ≈80 K at $z = 8.4$. While this is perhaps somewhat cooler than the $T_{\rm S} \gg T_{\rm CMB}$ regime, this contrast still amounts to only a ≈30% decrease in the 21 cm brightness temperature, and will be even less of an effect at $z \approx 7$ where the R15 model predicts 50% ionization.

6. CONCLUSIONS

We have interpreted new 21 cm power spectrum measurements from PAPER with a semi-analytic modeling framework. Using `21cmFAST` to cover the parameter space of cold reionization scenarios (i.e., where the hydrogen spin temperature is significantly below the CMB temperature during reionization), we find that power spectra with amplitudes above $\sim 100-1000$ mK^2 are generically produced for a wide range of neutral fractions, effectively independent of the other physical parameters during reionization. We cover the 2D ($T_{\rm S}$, $x_{\rm H\,I}$) space with a suite of simulations, and find that the PAPER measurements rule out spin temperatures below ≈5 K for neutral fractions between 10% and 85%. More stringently, if the universe is between 15% and 80% neutral at $z = 8.4$, we rule out spin temperatures below ≈7 K, and for neutral fractions between 30% and 70%, we require $T_{\rm S}$ to be greater than ≈10 K. Given the recent measurements from *Planck*, which suggest the midpoint of reionization occurs at $z = 8.8^{+1.7}_{-1.4}$ (Planck Collaboration et al. 2015), it is probable that the stronger lower bound of $T_{\rm S} > 10$ K applies. (Using an extended model of reionization, R15 predict the universe to be ≈70% neutral at $z = 8.4$, which would slightly lower our bounds on $T_{\rm S}$.)

We also explore a range of models for predicting the amount of heating the observed high-redshift galaxy population provides by $z = 8.4$. We find that the observed galaxy population can generally heat the gas above 10 K and, thus, is not constrained by the PAPER measurements. However if the star formation rate density $\dot{\rho}_{\rm SFR}$ drops off very steeply with redshift (as suggested by; e.g., Bouwens et al. 2015 and Oesch et al. 2014) and the correlation between X-ray luminosity and star formation rate is close to the locally observed value of $f_{\rm X} = 0.2$, we find that additional heating of the IGM beyond that provided by the observed galaxies is required. If the X-ray emission from high-redshift galaxies has fewer low-energy photons than expected and the IGM is heated less-efficiently, our constraints tighten considerably, ruling out all scenarios with either a steep redshift evolution in $\dot{\rho}_{\rm SFR}$ or a low value of $f_{\rm X}$.

Lastly, we considered the predicted X-ray heating of the IGM that would be expected under the reionization model of Robertson et al. (2015). This model produces an optical depth to the CMB in good agreement with the new *Planck* measurements (Planck Collaboration et al. 2015), and completes reionization by $z \approx 6$. We find that for all combinations of heating parameters, this model heats the IGM above the lower limit set by PAPER and, for our fiducial heating model, results in a spin temperature well above the CMB temperature. Therefore, the current lower limit on $T_{\rm S}$ set by PAPER is consistent with the R15 model, but does not require more high redshift star formation than that suggested by galaxy and CMB observations alone.

The potential for future 21 cm studies is also clear from Figure 4. With each increase in sensitivity, each new 21 cm measurement will rule out more of the ($T_{\rm S}$, $x_{\rm H\,I}$) parameter space. Figure 7 suggests that a spin temperature lower limit of ≈15 K would begin to rule out low efficiency X-ray heating models otherwise consistent with the R15 star formation rate density history; comparison with Figure 4 shows that placing a lower limit of this scale should require our a power spectrum spectrum upper limit to improve by only a factor of ≈2 (in units of mK^2). And, with an order of magnitude more sensitivity (again, in power units—only a factor of ≈3 in brightness sensitivity), 21 cm studies will begin to constrain the properties of the first galaxies (Pober et al. 2014; Greig & Mesinger 2015). PAPER has collected data with its full 128-element array for two seasons (double both the amount of data and number of antennas used to produce the constraints in this work), and the Hydrogen Epic of Reionization Array (Pober et al. 2014) has broken ground and will begin operations in a few years. With the continuing increase in the sensitivity of 21 cm measurements, we can expect to learn much more about the high-redshift universe in the near future.

PAPER is supported by grants from the National Science Foundation (NSF; awards 0804508, 1129258, and 1125558). J.C.P., A.R.P., and D.C.J. would like to acknowledge NSF support (awards 1302774, 1352519, and 1401708, respectively). J.E.A. would like to acknowledge a generous grant from the Mount Cuba Astronomical Association for computing resources. We graciously thank SKA-SA for onsite infrastructure and observing support. In addition we would like to thank our South African interns Monde Manzini and Ruvano Casper from Durban University of Technology (DUT), who helped build out the array from 32 antennas to the 64 antennas this analysis was based on. The authors would also like to thank Anson D'Aloisio, Adam Lidz, Jordan Mirocha, and Jonathan Pritchard for very helpful and fruitful conversations, Brant Robertson for providing the quantitative error contours in the R15 model, and our reviewer for helpful suggestions for better quantifying the effects of certain approximations in our work.

REFERENCES

Ali, Z. S., Zaki, S., Parsons, A. R., Zheng, H., et al. 2015, ApJ, 809, 61
Bouwens, R. J., Illingworth, G. D., Oesch, P. A., et al. 2015, ApJ, 803, 34
Bowman, J. D., Cairns, I., Kaplan, D. L., et al. 2013, PASA, 30, 31
Chen, X., & Kamionkowski, M. 2004, PhRvD, 70, 043502
Choudhury, T. R., Ferrara, A., & Gallerani, S. 2008, MNRAS, 385, L58
Christian, P., & Loeb, A. 2013, JCAP, 9, 14
Cowie, L. L., Barger, A. J., & Hasinger, G. 2012, ApJ, 748, 50
Dijkstra, M., Gilfanov, M., Loeb, A., & Sunyaev, R. 2012, MNRAS, 421, 213
Dillon, J. S., Liu, A., & Tegmark, M. 2013, PhRvD, 87, 043005
Dillon, J. S., Liu, A., Williams, C. L., et al. 2014, PhRvD, 89, 023002
Evoli, C., Mesinger, A., & Ferrara, A. 2014, JCAP, 11, 24
Fan, X., Strauss, M. A., Richards, G. T., et al. 2006, AJ, 131, 1203
Fialkov, A., Barkana, R., & Visbal, E. 2014, Natur, 506, 197
Field, G. B. 1958, PIRE, 46, 240
Finkelstein, S. L., Papovich, C., Ryan, R. E., et al. 2012, ApJ, 758, 93
Fragos, T., Lehmer, B., Tremmel, M., et al. 2013, ApJ, 764, 41
Furlanetto, S. R. 2006, MNRAS, 371, 867
Furlanetto, S. R., Oh, S. P., & Briggs, F. H. 2006, PhR, 433, 181
Furlanetto, S. R., & Stoever, S. J. 2010, MNRAS, 404, 1869
Gilfanov, M., Grimm, H.-J., & Sunyaev, R. 2004, MNRAS, 347, L57
Gnedin, N. Y., & Shaver, P. A. 2004, ApJ, 608, 611
Greig, B., & Mesinger, A. 2015, arXiv:1501.06576
Grimm, H.-J., Gilfanov, M., & Sunyaev, R. 2003, MNRAS, 339, 793
Hibon, P., Malhotra, S., Rhoads, J., & Willott, C. 2011, ApJ, 741, 101
Kuhlen, M., & Faucher-Giguère, C.-A. 2012, MNRAS, 423, 862
Larson, D., Dunkley, J., Hinshaw, G., et al. 2011, ApJS, 192, 16
Lehmer, B. D., Alexander, D. M., Bauer, F. E., et al. 2010, ApJ, 724, 559

Lidz, A., Zahn, O., McQuinn, M., Zaldarriaga, M., & Hernquist, L. 2008, ApJ, 680, 962
Liu, A., & Tegmark, M. 2011, PhRvD, 83, 103006
Lonsdale, C. J., Cappallo, R. J., Morales, M. F., et al. 2009, IEEEP, 97, 1497
Madau, P., & Dickinson, M. 2014, ARA&A, 52, 415
McGreer, I. D., Mesinger, A., & D'Odorico, V. 2015, MNRAS, 447, 499
McLeod, D. J., McLure, R. J., Dunlop, J. S., et al. 2015, MNRAS, 450, 3032
McQuinn, M., & O'Leary, R. M. 2012, ApJ, 760, 3
McQuinn, M., Zahn, O., Zaldarriaga, M., Hernquist, L., & Furlanetto, S. R. 2006, ApJ, 653, 815
Mesinger, A., Ewall-Wice, A., & Hewitt, J. 2014, MNRAS, 439, 3262
Mesinger, A., & Furlanetto, S. 2007, ApJ, 669, 663
Mesinger, A., Furlanetto, S., & Cen, R. 2011, MNRAS, 411, 955
Mineo, S., Gilfanov, M., & Sunyaev, R. 2011, AN, 332, 349
Mineo, S., Gilfanov, M., & Sunyaev, R. 2012a, MNRAS, 419, 2095
Mineo, S., Gilfanov, M., & Sunyaev, R. 2012b, MNRAS, 426, 1870
Morales, M. F., & Wyithe, J. S. B. 2010, ARA&A, 48, 127
Oesch, P. A., Bouwens, R. J., Illingworth, G. D., et al. 2014, arXiv:1409.1228
Ouchi, M., Shimasaku, K., Furusawa, H., et al. 2010, ApJ, 723, 869
Paciga, G., Albert, J. G., Bandura, K., et al. 2013, MNRAS, 433, 639
Pacucci, F., Mesinger, A., Mineo, S., & Ferrara, A. 2014, MNRAS, 443, 678
Parsons, A. R., Backer, D. C., Foster, G. S., et al. 2010, AJ, 139, 1468
Parsons, A. R., Liu, A., Aguirre, J. E., et al. 2014, ApJ, 788, 106
Parsons, A., Pober, J., McQuinn, M., Jacobs, D., & Aguirre, J. 2012a, ApJ, 753, 81
Parsons, A. R., Pober, J. C., Aguirre, J. E., et al. 2012b, ApJ, 756, 165
Planck Collaboration et al. 2015, arXiv:1502.01589
Pober, J. C., Liu, A., Dillon, J. S., et al. 2014, ApJ, 782, 66
Pober, J. C., Parsons, A. R., Aguirre, J. E., et al. 2013, ApJL, 768, L36
Pritchard, J. R., & Furlanetto, S. R. 2007, MNRAS, 376, 1680
Pritchard, J. R., & Loeb, A. 2008, PhRvD, 78, 103511
Pritchard, J. R., & Loeb, A. 2012, RPPh, 75, 086901
Ranalli, P., Comastri, A., & Setti, G. 2003, A&A, 399, 39
Robertson, B. E., Ellis, R. S., Furlanetto, S. R., & Dunlop, J. S. 2015, ApJ, 802, 19
Robertson, B. E., Furlanetto, S. R., Schneider, E., et al. 2013, ApJ, 768, 71
Shull, J. M., & van Steenberg, M. E. 1985, ApJ, 298, 268
Sobacchi, E., & Mesinger, A. 2014, MNRAS, 440, 1662
Tegmark, M. 1997, PhRvD, 55, 5895
Tilvi, V., Rhoads, J. E., Hibon, P., et al. 2010, ApJ, 721, 1853
Tingay, S. J., Goeke, R., Bowman, J. D., et al. 2013, PASA, 30, 7
Valdés, M., & Ferrara, A. 2008, MNRAS, 387, L8
van Haarlem, M. P., Wise, M. W., Gunst, A. W., et al. 2013, A&A, 556, A2
Volonteri, M., & Gnedin, N. Y. 2009, ApJ, 703, 2113
Wouthuysen, S. A. 1952, AJ, 57, 31
Yatawatta, S., de Bruyn, A. G., Brentjens, M. A., et al. 2013, A&A, 550, A136
Zahn, O., Mesinger, A., McQuinn, M., et al. 2011, MNRAS, 414, 727
Zheng, H., Tegmark, M., Buza, V., et al. 2014, MNRAS, 445, 1084